JOURNAL OF SPACECRAFT AND ROCKETS
Vol. 33, No. 4, July–August 1996

Numerical Study of Spacecraft Contamination and Interactions by Ion-Thruster Effluents

R. I. Samanta Roy* and D. E. Hastings†
Massachusetts Institute of Technology, Cambridge, Massachusetts 02139
and
N. A. Gatsonis‡
Worcester Polytechnic Institute, Worcester, Massachusetts 01609

A two-dimensional axisymmetric model was developed to investigate the plasma environment induced by an ion thruster and to assess plume backflow contamination. Predictions of the propellant charge-exchange plasma and sputtered molybdenum-grid metal effluents from the NASA 30-cm xenon ion thruster over a wide range of operating conditions during space operation are presented and discussed. It is verified that previous scaling relationships for the backflowing contamination, for a given geometry configuration, can be used to scale backflowing currents as a function of thruster operating conditions. The deposition of sputtered molybdenum-grid ions is computed and is found to be less than previous estimates. It is shown that the electron temperature plays an important role in the plume, with the backflow currents increasing with electron temperature. In addition, the effectiveness of a plume shield in reducing backflow contamination is assessed and found to be effective.

Nomenclature

A_g = sputtered grid area, m^2
A_n = grid neutral flow through area, m^2
$\bar{C}$ = average neutral speed, m/s
e = electron charge, C
I_b = thruster beam ion current, A
j_{bi} = beam ion current density, A/m^2
k = Boltzmann's constant (mks)
$\mathcal{M}$ = molecular weight, kg/mole
$m_{e,i}$ = electron, ion mass, kg
$\dot{m}_T$ = thruster total mass flow rate, kg/s
$\dot{N}$ = charge-exchange ion production rate, m^{-3} s^{-1}
$\mathcal{N}_A$ = Avogadro's number
n_{bi} = beam ion density, m^{-3}
$n_{i,e,n}$ = total ion, electron, neutral density, m^{-3} (a further subscript 0 denotes reference)
p_e = electron pressure, N/m^2
Q_e = electron heating term, W/m^3
R_c = radius of curvature of grids, m
r_T = thruster radius, m
T_e = electron temperature, K
T_w = thermal wall temperature of neutrals, K
$v_{bi,e}$ = beam ion, electron drift velocity, m/s
α = beam divergence angle, rad
Γ_s = sputtered-grid material flux, m^{-2} s^{-1}
η_p = propellant utilization efficiency
κ_e = electron thermal conductivity, W/m K
σ_{cex} = charge-exchange cross section, m^2
Φ_b = beam acceleration voltage, V
ϕ = electric potential, V
χ = charge-exchange ion production scaling factor

Received May 23, 1995; revision received Feb. 15, 1996; accepted for publication Feb. 16, 1996.

*Postdoctoral Associate, Space Power and Propulsion Laboratory, Department of Aeronautics and Astronautics; currently Research Staff Member, Institute for Defense Analyses, Alexandria, VA 22311. Member AIAA.

†Professor, Space Power and Propulsion Laboratory, Department of Aeronautics and Astronautics. Associate Fellow AIAA.

‡Assistant Professor, Mechanical Engineering Department. Member AIAA.

Introduction

TO confidently integrate electric propulsion thrusters such as ion thrusters into spacecraft, it is vitally important to assess their backflow contamination potential. We have developed a two-dimensional axisymmetric model of an ion-thruster plume to compute backflow contamination. In a companion paper,[1] we presented the motivation for this study and the details of the physical formulation and numerical model. In this paper, we employ the model to study the plume structure and backflow contamination of the current NASA 30-cm xenon ion thruster.

Physical Model

The ion-thruster plume and backflow contamination model used in this study, detailed in the companion paper,[1] takes into account the five major thruster effluents: 1) fast (>10 km/s) propellant beam ions that provide the thrust, 2) un-ionized propellant neutrals with thermal energies that flow from both the discharge chamber and the neutralizer, 3) slow (initially thermal) propellant ions created predominantly from charge-exchange (CEX) collisions between the beam ions and neutrals, 4) nonpropellant efflux (NPE) that consists mainly of eroded grid material, typically molybdenum, of which a fraction is charged by either CEX or electron bombardment ionization, and 5) electrons. We will consider each of these species. The focus of our model is the production of propellant and NPE ions within the beam, and their transport outward.

Beam Ions

The thruster grid is assumed to be a spherical segment of radius r_T (convex side downstream), with the velocities of the beam ions normal to the surface. Hence, the ions appear to be leaving a point source located at a distance R_c (the radius of curvature of the grids) behind the thruster exit plane. The velocity of the singly charged beam ions of mass m_i is expressed as $v_{bi} = (2e\Phi_b/m_i)^{1/2}$. The radial current density profile of the collimated beam ions [given in spherical polar coordinates (R, θ) for simplicity] is taken to be approximated by a parabolic axisymmetric profile given by

$$j_{bi}(R,\theta) = ev_{bi}n_{bi0}(R_c/R)^2[1 - (\theta^2/\alpha^2)] \quad (1)$$

which is a good approximation for modern thrusters.[2,3] This parabolic profile in the core of the beam is smoothed at the edges with an exponential decay. Given the beam ion current density, the beam ion density is then determined by

$$n_{bi}(r, z) = \frac{j_{bi}(r, z)}{e v_{bi}} \tag{2}$$

The effect of doubly ionized ions is neglected, since their density, depending on thruster operating conditions, is at most an order of magnitude less than that of the singly charged ions.

Neutral Model

The propellant that remains un-ionized in the thruster effuses out from the discharge chamber and exits through the grids in free-molecular flow with a temperature close to that of the thruster discharge-chamber walls, typically around 500 K for thrusters using xenon. The average neutral density right at the thruster grids is determined from the beam ion current and the propellant utilization efficiency by the relation

$$n_{n0} = \frac{4 I_b}{e \bar{C} A_n}\left(\frac{1-\eta_p}{\eta_p}\right) \tag{3}$$

where $\bar{C}$ is the mean thermal speed given by $(8kT_w/\pi m_i)^{1/2}$. The propellant utilization efficiency is based on the total neutral flow rate (discharge + neutralizer):

$$\eta_p = (I_b/\dot{m}_T)(m_i/e) \tag{4}$$

The neutral density field is modeled as the flow from a single point source that is located one thruster radius behind the exit plane of the grids. The neutral gas density[1] is given by

$$n_n(R, \theta) = a(n_{n0}/2)\left\{1 - \left[1 + (r_T/R)^2\right]^{-\frac{1}{2}}\right\}\cos\theta \tag{5}$$

where $a = (1-1/\sqrt{2})^{-1}$ is a correction factor to allow for the shifting of the point source and $R = [r^2+(z+r_T)^2]^{1/2}, \theta = \tan^{-1}[r/(z+r_T)]$.

CEX Propellant Ions

Slow propellant ions are created both within the thruster grids and downstream inside the beam by resonant CEX collisions of the following type between the fast beam ions and the slow thermal neutrals (e.g., for xenon):

$$Xe^+_{fast} + Xe^0_{slow} \rightarrow Xe^+_{slow} + Xe^0_{fast} \tag{6}$$

The spatial volumetric production rate of CEX ions is given by

$$\dot{N}_{cex}(\boldsymbol{x}) = n_n(\boldsymbol{x}) n_{bi}(\boldsymbol{x}) v_{bi} \sigma_{cex}(v_{bi}) \tag{7}$$

where the relative collision velocity is taken to be the beam ion velocity. For plume electron temperatures around 1–2 eV, common in xenon ion thrusters, CEX is the dominant ion production mechanism rather than electron impact ionization.[1] In general, CEX production rates are low enough that the beam and neutral densities can be taken to be fixed quantities.

NPE

Neutral molybdenum, sputtered mainly from the accelerator grid, can become ionized in the plume and flow back towards the spacecraft, presenting a serious contamination hazard due to its low vapor pressure. The neutral density is computed from the sputtered material flux, which is estimated from grid mass-loss measurements. Given that an amount of mass M is lost over a period of time τ, the average flux is

$$\Gamma_s = (M/\tau A_g)(\mathcal{N}_A/\mathcal{M}) \tag{8}$$

The spatial distribution of the sputtered neutrals is assumed to be a cosine distribution as described by Eq. (5). The ejection energy distribution of molybdenum is close to Maxwellian, and the density is found by dividing the sputtered flux by the most probable ejection speed.[1] The neutral molybdenum can become ionized via CEX and electron impact—the latter being important at electron temperatures above 1.5 eV.

Electrons

The electrons emitted from the neutralizer on the thruster are modeled as a local Boltzmann distribution with a spatially varying temperature $T_e(\boldsymbol{x})$:

$$n_e(\boldsymbol{x}) = n_{e\infty}\exp\left[\frac{e\phi(\boldsymbol{x})}{kT_e(\boldsymbol{x})}\right]. \tag{9}$$

The electron temperature is determined by solving the electron energy equation,

$$\tfrac{3}{2} n_e \boldsymbol{v}_e \cdot \nabla k T_e + p_e \nabla \cdot \boldsymbol{v}_e = -\nabla \cdot \boldsymbol{q}_e + Q_e \tag{10}$$

where $\boldsymbol{q}_e = -\kappa_e \nabla T_e$ is the conductive heat flux and $p_e = n_e k T_e$. The electron heating term Q_e is due to collisional transfer and ohmic heating. The electron drift velocity is taken to be the beam ion velocity inside the beam, and zero outside. The electrons, as well as the ions, are unmagnetized in the model.

Numerical Implementation

Figure 1 shows a schematic of the general computational domain, which includes a model spacecraft with optional solar-array panels. Typical axisymmetric domain sizes are 1–3 m. All surfaces of the spacecraft are either biased at fixed potentials or allowed to float as a single isolated conductor. An optional plume shield can be included to investigate its effect on reducing the backflow. The beam-ion and neutral-propellant models developed give the beam properties in the region of the plume, and the volumetric CEX propellant-ion production model is used to determine the number of propellant CEX ions that are created per unit time per unit volume within the plume. To model the expansion of the CEX ions, a hybrid electrostatic plasma particle-in-cell (PIC) technique is employed. The PIC method follows the propellant CEX ions under the influence of self-consistent electric fields as they are transported out of the beam and form a plasma cloud that surrounds the spacecraft. Electrons from the neutralizer are not treated as particles but are described by the fluid model expressed by Eq. (9). The NPE ions are also created volumetrically—either by CEX or by ionization at higher electron temperatures. However, because the NPE ion density is much smaller than the propellant plasma densities, the effect on the potential is negligible. Hence, the NPE plasma propagation is determined solely by ion tracking in the potential determined from the propellant CEX ion expansion.

The simulation is run until steady state is achieved, when the number of particles within the domain becomes constant, i.e., the loss of particles at the boundaries and spacecraft surfaces balances the production rate within the plume. At steady state, the current backflowing to biased spacecraft surfaces due to propellant CEX and NPE ions can be computed, and assessments of surface deposition can be made. In this work, the surfaces are assumed to be absorbing. The nonlinear Poisson equation for the potential and the nonlinear electron temperature equation (which is strongly elliptic) are both solved throughout the computational domain. The far right, top, and far left upper boundaries shown in Fig. 1 are left open to space, although their potentials can be fixed to simulate a

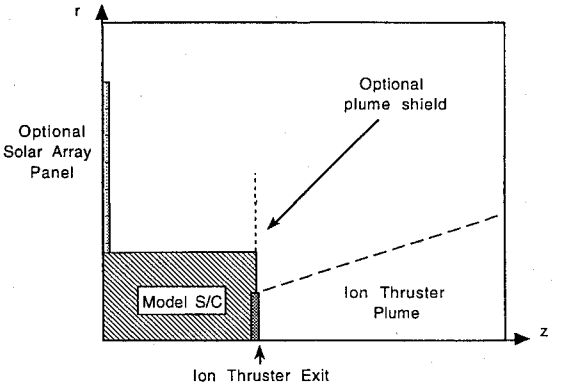

Fig. 1 Schematic of computational domain.

ground testing chamber. At the thruster front, the electron temperature is fixed according to experimental measurements. The lower boundary of the domain in front of the spacecraft is the plume centerline; particles that reach this boundary are reflected. A uniform background plasma density is assumed. Because the thruster-produced plasma environment is orders of magnitude larger than the ambient, we ignore the dynamics of the background plasma over the length scales of interest.

Results

Contamination Predictions for the NASA 30-cm Xe Ion Thruster

In this section, the backflow contamination is examined for the NASA 30-cm thruster that was developed as an element in the NASA Solar Electric Propulsion Technology Applications Readiness (NSTAR) program. The thruster incorporates innovations in design, materials, and fabrication techniques. Specific development efforts included thruster design optimizations, component life testing and validation, vibration testing, and performance characterizations. However, thus far, no detailed plume measurements for backflow contamination have been conducted.[4,5] In this numerical study, emphasis is placed on determining scaling relationships between the backflow and the thruster operating conditions.

The operating envelope for the thruster is shown in Fig. 2. The beam current ranges from 0.5 to 3 A, the beam voltage ranges from 550 to almost 1400 V, and the input power envelope ranges from 0.5 to 4.9 kW. The black circles represent operating conditions used in NASA–Jet Propulsion Laboratory (JPL) tests,[6] and the white squares represent those mapped out by NASA Lewis Research Center (LeRC).[5] The solid curve drawn at the bottom of the envelope is the thruster perveance limit (space-charge limit of the grids). For a fixed voltage, the current cannot be increased above the space-charge-limited flow value.

In this paper, all six of the JPL operating points and a subset of the LeRC operating points are studied. Points from the LeRC envelope are chosen that will enable scalings to be studied. Thus, points of constant voltage of 1090 V, points of constant current of 1.1 A, and the extreme limits of the operating envelope are examined. The specifics of the JPL operating points are given in Table 1, and those of the NASA LeRC points in Table 2.

JPL Operating Points

The rationale for the JPL power throttling operating points shown in Table 1 is that the maximum-power point is set to be the minimum

Table 1 NASA 30-cm xenon thruster: JPL operating points[6]

Point no.	Power, kW	I_b, A	Φ_b, V	v_{bi}, m/s	η_p	$\dot{m}$, mg/s	Thrust, mN	I_{sp}, s
J1	0.497	0.5	676	31,500	0.71	0.96	20	2177
J2	0.996	0.72	1107	40,300	0.75	1.31	38	2929
J3	1.132	0.81	1119	40,500	0.81	1.36	43	3194
J4	1.521	1.15	1075	39,700	0.84	1.87	59	3238
J5	1.652	1.23	1100	40,200	0.88	1.9	64	3450
J6	2.304	1.74	1100	40,200	0.89	2.67	91	3477

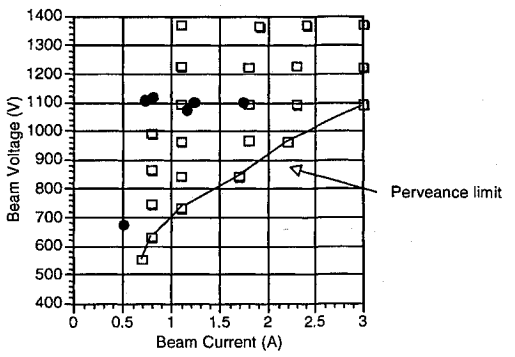

Fig. 2 Operating envelope of NSTAR ion thruster: •, JPL[6] and □, LeRC[5].

Table 2 NASA 30-cm xenon thruster: LeRC operating points[5]

Point no.	Power, kW	I_b, A	Φ_b, V	v_{bi}, m/s	η_p	$\dot{m}$, mg/s	Thrust, mN	I_{sp}, s
L1	0.7	0.7	552	28,459	0.78	1.23	28	2290
V1	1.12	1.1	730	32,728	0.85	1.76	46	2680
V2	1.26	1.1	843	35,170	0.85	1.76	50	2920
V3	1.4	1.1	963	37,590	0.85	1.76	54	3150
V4, I1	1.56	1.1	1093	40,047	0.85	1.76	59	3400
V5	1.73	1.1	1227	42,431	0.85	1.76	62	3630
V6, L2	1.9	1.1	1372	44,868	0.85	1.76	67	3860
I2	2.43	1.8	1094	40,065	0.85	2.88	95	3370
I3	3.05	2.3	1091	40,010	0.82	3.83	122	3250
I4, L3	3.88	3.0	1090	39,992	0.91	4.5	154	3470
L4	4.88	3.0	1371	44,851	0.91	4.5	178	4030

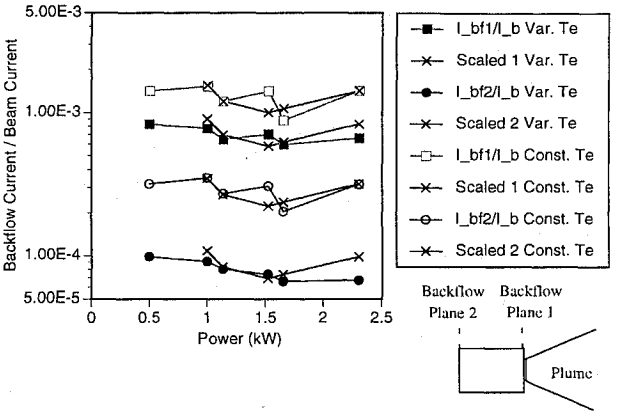

Fig. 3 NSTAR backflow current for JPL operating conditions.

power necessary to provide significant benefit for small-body rendezvous missions. The other points are selected to maximize thruster efficiency under the constraints of the propellant feed system design. The numerical simulation model is applied to these six operating points for both variable and constant temperature. The constant-temperature model does not involve the solution of the electron energy equation (10), and hence is more computationally efficient for parametric studies. The role of the electron temperature has been discussed in Ref. 1. In that work, comparisons with data show that the isothermal model yields higher, more conservative values for the backflow than the variable-temperature model. Ambient conditions appropriate to the low Earth orbit environment were used, with a background plasma density of 10^{10} m^{-3}, an ambient electron temperature of 0.1 eV, and no neutral background pressure. The computational domain was 1×1 m, and the thruster body was taken to be 50 cm long and 20 cm in half width. The beam divergence angle was taken to be 20 deg, and the neutral propellant grid transparency ratio was 0.24. The spacecraft or thruster body was assumed to have a floating potential of -1 V, and the beam electron temperature at the thruster exit was set to 5 eV, although only CEX collisions were included. This higher electron temperature will give a more conservative estimate of the backflow. Later in this paper, we will examine the sensitivity of the plume backflow to beam electron temperature.

The backflow current was computed on two planes extending from the top of the thruster body. One plane is located at the thruster exit plane (plane 1) and another at $z = 0$ (plane 2). The planes are separated by 50 cm, and the radial height of the planes is 80 cm. These planes do not represent any typical physical configuration but were chosen so that a large enough variation in the backflow could be seen. In Fig. 3, the ratio of the computed backflow current on the two planes to the beam current as a function of the thruster operating power (points J1–J6) is shown. Results for both the variable- and the constant-temperature models are shown.

As can be seen in Table 1, a wide range of thruster operating conditions (i.e., I_b, η_p, and Φ_b) is covered as the power is throttled from 0.5 to 2.3 kW. Kaufman and Carruth[7] proposed a scaling relationship for the CEX propellant ion backflow that is based on the

CEX ion production rate, which is proportional to the beam ion and neutral densities and is given by

$$\dot{N}_{\text{cex}} \sim I_b^2[(1-\eta_p)/\eta_p)]\sigma_{\text{cex}}(v_{bi}) = \chi \tag{11}$$

This relationship was validated by applying the scaling factor to the numerical results. To do so, given χ and the backflow current for the first point, the backflow current for any other point i, I_{bfi}, is computed by multiplying the backflow current of the first point by χ_i/χ_1:

$$I_{\text{bfi}} = I_{\text{bf1}}(\chi_i/\chi_1) \tag{12}$$

This procedure has been applied, and the results are overlaid on Fig. 3, where the $\times$ symbols indicate the scaled predictions of the backflow current that have been normalized by the beam current. As an example, with the variable-temperature model, the backflow current over plane 1 for point J1 is 4.13×10^{-4} A, and $\chi_1 = 0.3995$. For point J3, $\chi_3 = 0.5459$ and the predicted backflow current is found to be $(0.5459/0.3995)(4.13 \times 10^{-4}) = 5.6 \times 10^{-4}$ A. The numerical result with the variable-temperature model is 5.3×10^{-4} A, which is very close. Figure 3 demonstrates that this scaling relationship is in good agreement with numerical predictions. From Fig. 3, it appears that the ratio of the backflow current to the beam current is almost constant as a function of power. However, the propellant utilization efficiency is also changing.

Figure 3 shows that the isothermal-model values are almost twice those of the variable model at plane 1, and about three times at plane 2. The spatial distributions of the CEX ions are different for the two temperature models also. The variable-temperature model gives a faster decay in the current, as can be seen by comparing the currents crossing planes 1 and 2. The current crossing plane 2 is about 8–9 times less than that crossing plane 1 for the variable-temperature model, but about 4–5 times less for the isothermal model. Note that the scaling relationship (11) is independent of the electron temperature but still follows the numerical results well for both constant- and variable-temperature models.

Thus far, scalings of a global quantity—the backflow current on various planes—have been examined. It should be expected that these currents scale with the rate of CEX ion production, as required for continuity. However, the structure of the backflow field must be examined as the thruster is throttled through various operating conditions. Figures 4 and 5 depict the CEX plasma density distributions computed with the variable-temperature model for all six operating points. Figure 4 shows a radial cut through the domain along a ray 100 deg from the plume centerline from a point 10 cm downstream

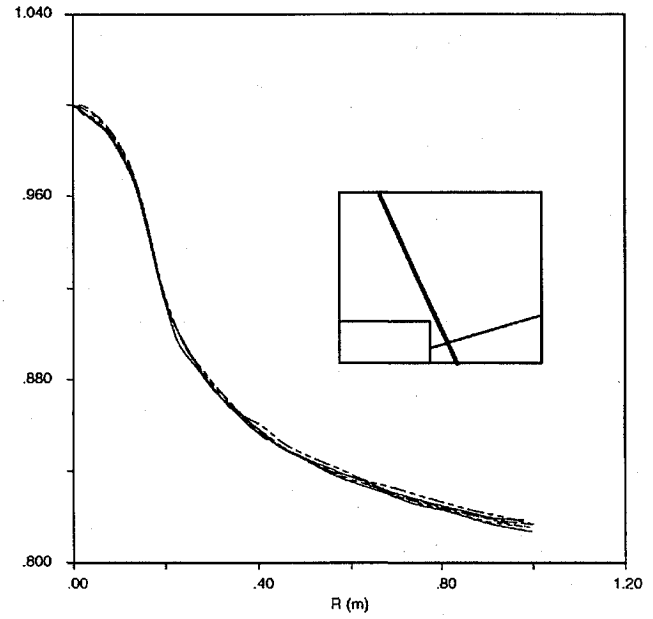

Fig. 4 Radial distribution of CEX plasma density. Two-dimensional plume simulation CEX distribution; six JPL points, variable T_e model, radial distribution along ray 100 deg from CL, origin of ray 10 cm from thruster front.

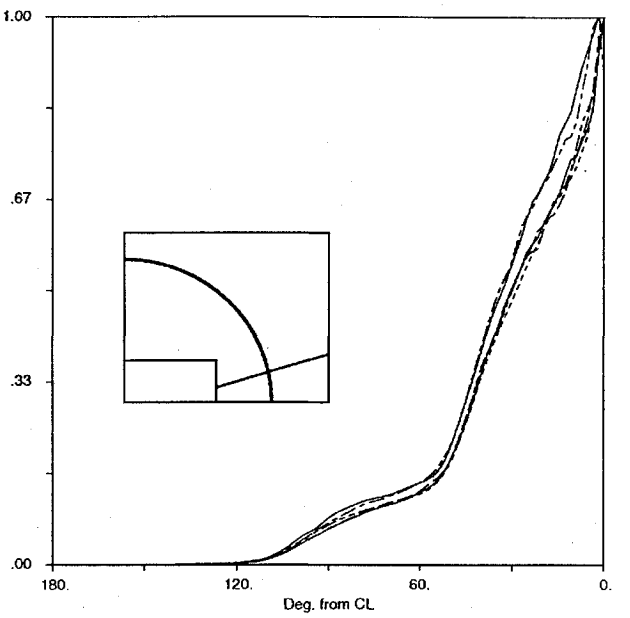

Fig. 5 Angular distribution of CEX plasma density. Two-dimensional plume simulation CEX distribution; six JPL points, variable T_e model, angular distribution at $r = 0.35$ from point 10 cm in front of thruster.

of the thruster face. The density has been normalized with the value of the density at the plume centerline ($\theta = 0$). Within the numerical noise of the PIC method, all six cases, spanning a power range of a factor of almost 5, appear to follow the same shape. Figure 5 shows the density distribution along an arc of radius 0.35 m from the same point 10 cm downstream of the thruster. The CEX density falls to zero at about $\theta = 145$ deg, where the top of the thruster body is intercepted. Figure 5 also shows that within a certain amount of scatter, the normalized distributions over an entire sweep of 145 deg are very similar.

In addition to the CEX ion density, the CEX ion current density distributions were examined in the same manner.[2] The distributions were essentially the same, despite larger fluctuations that were present because the current density is a weighting of both the particles' charge and their velocities. Simulations conducted with the isothermal model for both CEX ion density and current density yielded similar distributions for all six operating points. However, current densities predicted with the isothermal model were higher than with the variable temperature model.

An important conclusion from Figs. 4 and 5 is that the spatial distribution of the CEX plasma is fairly independent of the thruster operating conditions. Only the magnitude is dependent upon the beam current, propellant utilization efficiency, and other parameters, as shown in the scaling parameter χ that has been proposed.[7] It should be noted that slight variations in the spatial distribution of the CEX plasma predicted with the variable-temperature model may be caused by the influence of the temperature field on the potential. Over the operating envelope, the ion-to-neutral density ratio changes, which affects the thermal conductivity and consequently the electron temperature and the potential. However, these effects are not very significant. Note that these conclusions are for the given geometry, i.e., thruster or spacecraft size. One cannot use the scaling factor (11) to predict the backflow current if, say, the thruster body width is doubled.

NASA LeRC Operating Points

The NASA LeRC points shown in Table 2 have been categorized with alphabetical prefixes: I, V, and L. The four points with I are points of constant voltage, and the current is varied. The six points with V are points of constant current, and the voltage is varied. The four points with L are the four vertices of the thruster operating envelope. Some of the points have multiple labels, because they overlap in the envelope. For these parametric studies, only the isothermal model was used. All other variables from the JPL runs, aside from the operating conditions listed in the table, were used in the LeRC runs.

Table 3 Lower and upper limits to backflow contamination for LeRC points

Point	I_b, A	I_{bf1}/I_b	I_{bf2}/I_b
L1 (lower)	0.7	1.45×10^{-3}	3.20×10^{-4}
L4 (upper)	3.0	1.77×10^{-3}	4.05×10^{-4}

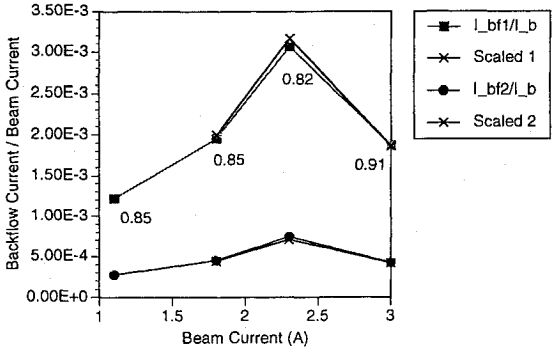

Fig. 6 Backflow current vs I_b. Numbers on upper points are propellent utilization efficiencies.

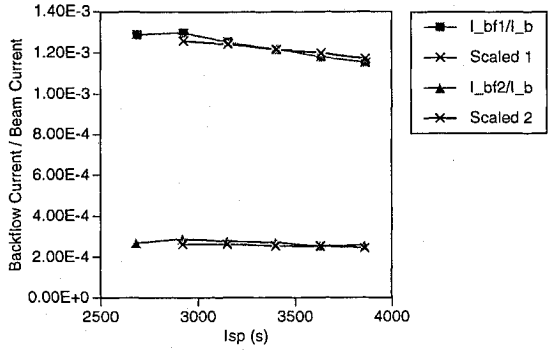

Fig. 7 Backflow current vs specific impulse (proportional to beam potential). Only voltage → beam ion velocity is being varied; constant beam current = 1.1 A and constant mass flow rate = 1.76 mg/s.

The backflow currents for variations in beam current for constant beam voltage were computed over the same two planes as in the JPL calculations. Figure 6 shows the ratio of the backflow current to the beam current as a function of the beam current with the beam voltage constant at 1090 ± 4 V. The scaling factor (11) has been used to predict the backflow currents based on the point I1, and these values are marked with the × symbol. There is very good agreement with this scaling relationship. The variations are not only due to changes in the beam current, but also due to changes in the propellant utilization efficiency.

In addition, the backflow current for constant beam current and mass flow rate (hence propellant utilization efficiency) was computed. In this case, only the beam voltage is varied, which changes only the CEX cross section. Figure 7 depicts the ratio of the backflow current to the beam current (1.1 A) as a function of the specific impulse (which is proportional to $\Phi_b^{1/2}$); it shows a slight decrease because the CEX cross section is weakly decreasing with increasing beam ion velocity. The scaling relationship (11) again gives good agreement.

Last, the backflow currents for the limits of the operating envelope are presented to show bounds on the backflow. Two limit points, L2 and L3, have been computed already as points V6 and I4, respectively. The other two points represent the upper and lower bounds on the power of the thruster. The backflow current values are shown in Table 3 for L1, the point with the lowest voltage and current, and L4, the point with the highest voltage and current. The ratios of the backflow currents to the beam currents are almost the same, but the scaling factor for L4 is about 5.56 times larger than for L1. Hence, the actual backflow current increases by a factor of 5.56 from the lowest to the highest power settings (a range of 7) for the 30-cm thruster.

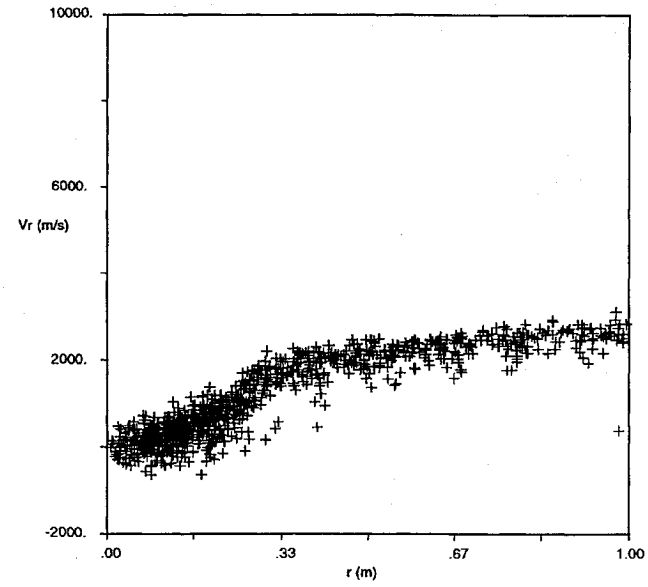

Fig. 8 Radial velocity vs radial position: phase-space plot for beam electron temperature of 1 eV.

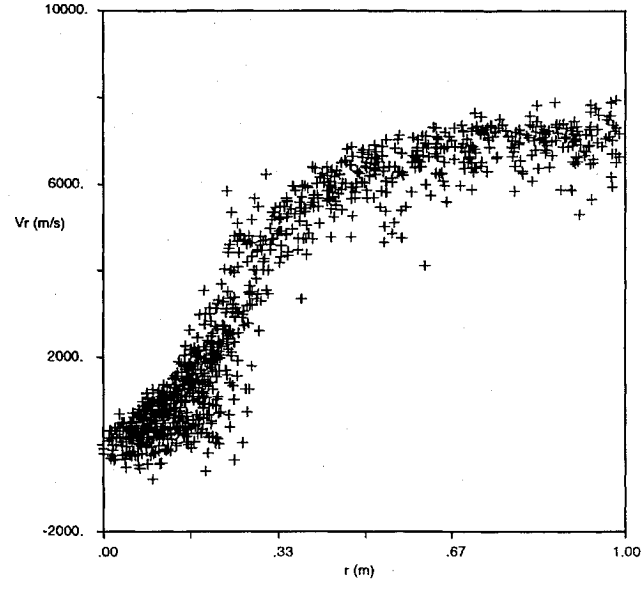

Fig. 9 Radial velocity vs radial position: phase-space plot for beam electron temperature of 5 eV.

Effect of Electron Temperature

The sensitivity of the backflow current to the electron temperature is investigated by examining JPL point J2 using the variable-temperature model with beam electron temperatures of 1 and 5 eV. As would be expected, since the potentials scale with the electron temperature, the higher electron temperature yields higher beam potential drops, and hence the CEX ions are accelerated to higher velocities. Figures 8 and 9 show phase-space plots of radial velocity vs radial position for the CEX ions with beam electron temperatures of 1 and 5 eV, respectively. For the 1-eV case, the maximum radial velocity is about 2500 m/s, corresponding to a beam potential drop of about 4 V. For the 5-eV case, the maximum radial velocity is about 7000 m/s, corresponding to a beam potential drop of about 33 V. Because of the higher velocities, the backflow current is increased. The integrated current flowing across plane 1 at the thruster exit is 2.3×10^{-4} A for the 1-eV case and 5.6×10^{-4} A for the 5-eV case. Across plane 2 at $z = 0$, the current values are 2.6×10^{-5} A for 1 eV and 6.5×10^{-5} A for 5 eV. Thus, the electron temperature in the beam, which physically is usually determined by the neutralizer coupling voltage, plays an important role in determining the magnitude of plume backflow. However, there is not an exact linear dependence of plume properties on the beam electron temperature, owing to nonlinear effects related to the electron thermal conductivity.[2]

Sputtered Grid Material

In this subsection, the transport of sputtered grid material from the NASA 30-cm xenon ion thruster is examined. Patterson et al.[5] estimated the in-space accelerator-grid mass loss rate for a number of operating conditions, and these values are shown in Table 4. The first point corresponds to point I1 (or V4) in Table 2, the second to point I2, and the third point is close to I3. Based on these mass loss rates, the neutral molybdenum density is computed using the model described previously.

Electron-impact ionization of the neutral molybdenum sputtered off the grids is important for electron temperatures as low as 1.5 eV (Ref. 1). In the calculations presented here, for each operating point, two cases were run for the creation of charged molybdenum. The high-rate case included ionization with an electron temperature of 5 eV, and the low-rate case considered only CEX collisions with the xenon ions (valid for electron temperatures near 1 eV or less). These two limits provide a bound on the creation of molybdenum ions. The trajectories of the created molybdenum ions are tracked in the potential fields computed from the propellant CEX ion expansion.[1]

In Fig. 10, the ratio of the molybdenum to the xenon CEX ion current density for the I3 point with high ion creation rate is shown. Within the beam, the ratio is about 10^{-4}; however, in the backflow region it is below 10^{-5}. The important point is that the molybdenum ion distribution is considerably different spatially than the xenon CEX ion distribution. In previous analytical models of molybdenum deposition, the spatial distribution of both species was assumed to be the same, only differing by a constant.[7] This assumption led to higher estimates of the molybdenum deposition and increased concern for spacecraft contamination. However, simulations show that in the backflow region the molybdenum density is noticeably less. The reason is the higher energy of the molybdenum ions, which makes them less likely to turn back towards the spacecraft. The most probable energy of the sputtered molybdenum is about 5 eV, the average being 15–20 eV. In contrast, the thermal xenon neutrals only have an energy around 0.02 eV (500 K). Figure 11 shows the trajectories of a typical xenon and a molybdenum ion released radially outward from the same point at the beam edge with energies

Table 4 Anticipated accelerator-grid erosion rates in space for NASA 30-cm xenon thruster[5]

Power, kW	Label (Table 2)	Mass loss, g/kh	Mo neutrals, m^{-3}
1.1	I1, V4	1.41	1.10×10^{13}
2.40	I2	2.89	2.25×10^{13}
3.41	Close to I3	4.18	3.250×10^{13}

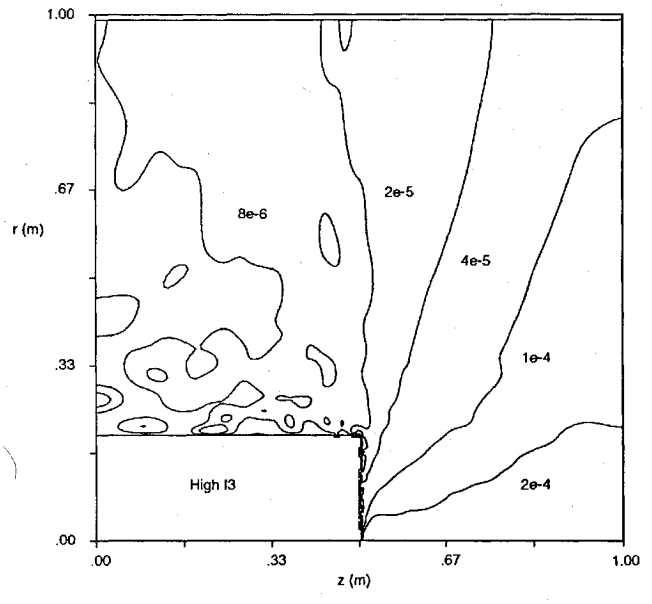

Fig. 10 Two-dimensional ion thruster plume simulation ratio of Mo to Xe CEX ion current density: high I3 case, T_e = 5 eV.

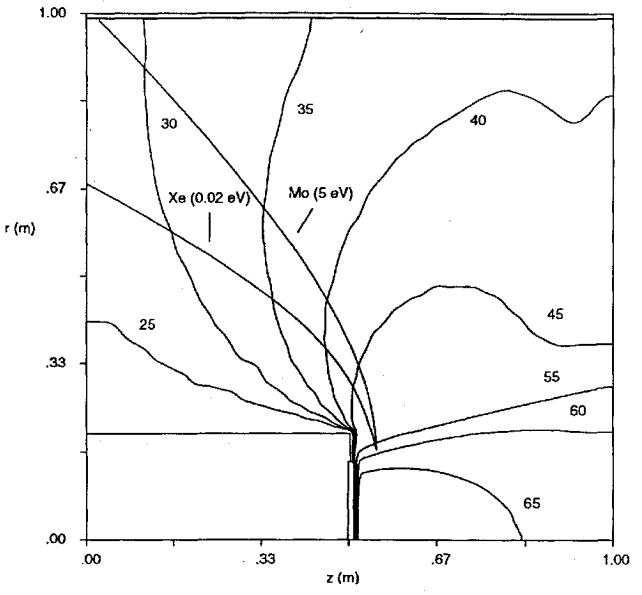

Fig. 11 Two-dimensional ion thruster plume simulation comparision of Xe and Mo trajectories: LeRC I3, T_e = 5 eV constant.

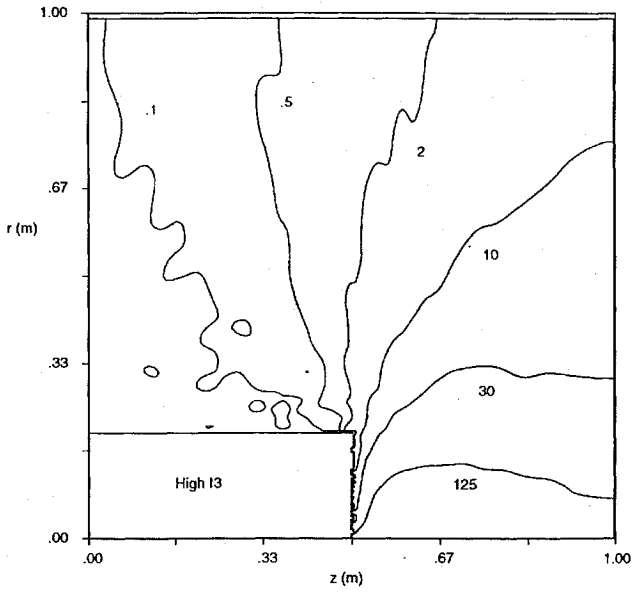

Fig. 12 Two-dimensional ion thruster plume simulation molybdenum deposition (monolayer/year): high I3 case, T_e = 5 eV (ionization).

of 0.02 and 5 eV, respectively, with the potential contours superimposed. It can be seen that the less energetic xenon ion is turned back more than the molybdenum ion. Hence, even in a case of equal Mo^+ and Xe^+ production rates, the density of the molybdenum in the backflow area will be less. In addition, the values in Fig. 10 show that neglecting the molybdenum ion density in Poisson's equation is a good approximation, since the density is negligible compared to the propellant ion density.

For contamination assessment of the molybdenum, the most important quantity of interest is the deposition rate. A useful unit is monolayers per year, assuming all the molybdenum sticks. In Fig. 12, a contour map of the deposition rate of the molybdenum ions is shown for the I3 case with high ion creation rate. These values, assuming normal impingement, are the ion current density converted to monolayers per year. Within the plume, the deposition rates do not take into account the neutral deposition, nor the fact that the deposition on a surface will be much lower because of sputtering by the energetic beam ions. However, in the backflow region, the deposition rate is solely due to the charged molybdenum, and is about 0.1 monolayer/year. As the thruster power is decreased, the grid mass loss decreases, and hence so does the molybdenum backflow.

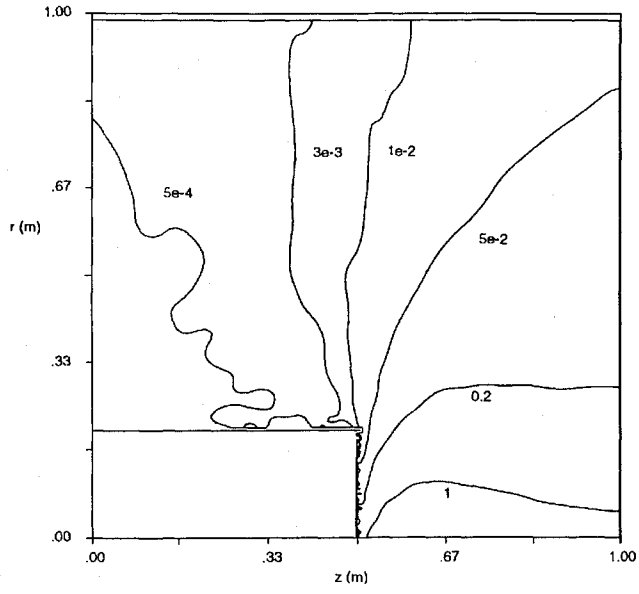

Fig. 13 Two-dimensional ion thruster plume simulation molybdenum deposition (monolayer/year): low V4 case, T_e = 1 eV (CEX).

Figure 13 shows the deposition rates for the I1 case with only CEX as the ion production mechanism. Here we see that the molybdenum deposition is only around 5×10^{-4} monolayer/year in the backflow region. (For the I1 case with electron-impact ionization, the value is around 2×10^{-2} monolayer/year.)

The neutral molybdenum density in Table 4 varies only by a factor of three over a power range of two. Because the molybdenum is sputtered by the propellant CEX ions impinging on the grid, it could be expected that the molybdenum density scales according to the scaling factor used for the propellant CEX ions. Using Eq. (11), the scaling factor is about 5.4, which is higher than the numerical value. The reason for this discrepancy is that the accelerator-grid voltage is changing, which affects the sputtering yield. The estimates[5] in Table 4 are based on experimental correlations of the grid voltage and the grid impingement current. Moreover, though the propellant CEX impingement current may increase by a factor of 5.4, the actual grid mass loss may not scale as such, because the material sputtered away is not all ejected completely from the grid but may redeposit elsewhere. It is therefore of interest to develop a scaling relationship between the molybdenum ion density and thruster operating conditions.

The creation rate of the molybdenum ions scales with the neutral molybdenum density, the beam ion density, and a function that depends on the particular collision process. For CEX collisions, this function is the product of the beam ion velocity and the cross section. For electron-impact ionization, this function is solely dependent upon the electron temperature. The neutral density scales with the sputtering rate (which is given), and the beam ion density scales with the ratio of the beam ion current to the beam ion velocity (the beam voltage). Thus, the creation of molybdenum ions due to CEX can be written as

$$\dot{N}_{\text{cex Mo}} \sim \Gamma_s (I_b / v_{bi}) v_{bi} \sigma (v_{bi}) \tag{13}$$

and the creation rate due to electron-impact ionization as

$$\dot{N}_{\text{ion Mo}} \sim \Gamma_s (I_b / v_{bi}) f(T_e) \tag{14}$$

Using these scaling factors, the relative molybdenum ion density in the backflow region between the three operating points can be determined. Notice that for the three operating points considered here, T_e is a constant, and the beam ion velocity is nearly constant. Therefore, the molybdenum deposition is expected to scale as the product of the sputtering loss rate and the beam current. In Fig. 14, the integral of the molybdenum current density over two planes is shown. Plane 1 is at the thruster exit, and plane 2 is located 0.5 m behind at $z = 0$. Both planes reach from the thruster top at $r = 0.2$ m to the upper domain boundary at $r = 1$ m. The backflow has been

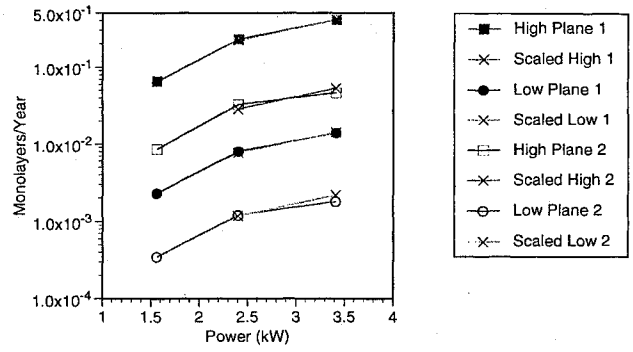

Fig. 14 Mo backflow current as a function of thruster power. Constant T_e = 5 eV; Low: CEX and High: e-ionization.

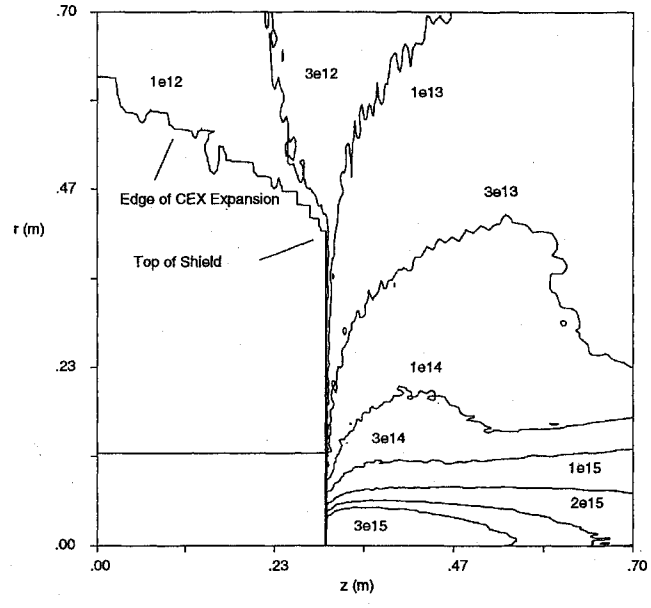

Fig. 15 Effect of plume shield on the CEX ion backflow. Total ion density (m^{-3}).

expressed in monolayers per year by integrating the current density to obtain the current, dividing by the area of the annulus over which the integration occurred [$\pi(1^2 - 0.2^2)$ m^2], and then converting to monolayers per year. Thus, this value is an average deposition, and is shown as a function of the thruster power for the three operating points and the high and low ion creation rates. Superimposed on the computational values are the scaled values from Eqs. (13) and (14) based on the point I1, which are marked with the × symbol. Therefore, even though the grid mass loss increases only by a factor of 3 from point I1 to I3, the beam current has increased by a factor of 2, and hence the molybdenum deposition increases by a factor of 6. The difference in deposition rates between the two ion creation bounds is very large, with electron-impact ionization yielding deposition rates 20–30 times larger than CEX ion creation. This observation again demonstrates the importance of the electron temperature in the plume. The serious effect of molybdenum deposition has been investigated,[8] and even a monolayer of molybdenum can cause serious degradation in the transmittance of solar-cell cover glasses.

Effect of a Plume Shield to Reduce Backflow

A possible way to reduce the backflow of ions from an ion thruster is to use a plume shield. In this section, this effect is demonstrated by placing a 30-cm-high plume shield of infinitesimal thickness at the thruster exit perpendicular to the plume axis, as shown in Fig. 1. To compare the shielded flowfield with experimental data on an unshielded thruster, a simulation of a 15-cm mercury thruster was performed. The constant-electron-temperature model was used, and the shield was biased to +5 V and was assumed to be completely absorbing.

Figure 15 shows the computed total propellant ion density, displaying the same contour levels as a computation without a plume shield (Fig. 6 of Ref. 1). It can be seen that in the backflow region behind the shield, the propellant CEX plasma is completely eliminated (and hence the molybdenum ions as well). In this ground test, the density of the background plasma was 10^{12} m^{-3}. Figure 15 shows a contour of value 10^{12} m^{-3} at the edge of the CEX cloud expansion. The plume shield is very effective in reducing any backflow contamination from the region behind the shield. However, the shield adds mass to the spacecraft structure, as well as possibly causing additional spacecraft contamination due to erosion. In any actual spacecraft–thruster integration process, the ratio of the mass of the shield to the effective area protected would have to be minimized. In addition, other shield shapes, such as a conical geometry, may be more effective.

Conclusions

A two-dimensional axisymmetric model of the backflow contamination of an ion-thruster plume was developed and applied to predict the backflow contamination of the NASA 30-cm xenon ion thruster over the operating envelope of the thruster. The CEX propellant backflow was computed, as well as the deposition of sputtered molybdenum from the thruster grids. A previously proposed scaling relationship for the propellant CEX ion backflow was verified and shown to be useful in scaling backflow contamination as a function of thruster operating conditions. The ratio of the xenon propellant to sputtered molybdenum ions was found not to be a constant throughout the backflow region, a commonly used assumption in previous studies. Hence, the molybdenum deposition is not as high as previously expected. The sensitivity of the plume backflow to the beam electron temperature was examined, and found to have a strong role due its effect on the CEX ion velocities. Last, a plume shield was evaluated and found to be effective in reducing the backflow.

Acknowledgments

R.I.S.R. was supported in part by a National Science Foundation Graduate Fellowship. Support for R.I.S.R. and D.E.H. is also acknowledged from the U.S. Air Force Office of Scientific Research, the Jet Propulsion Laboratory of the California Institute of Technology, and the Applied Physics Laboratory (APL) of Johns Hopkins University. N.A.G. was supported by APL. The authors would like to acknowledge useful discussions with Manuel Martinez-Sanchez of the Massachusetts Institute of Technology and Barry Mauk of APL.

References

[1]Samanta Roy, R. I., Hastings, D. E., and Gatsonis, N. A., "Ion-Thruster Plume Modeling for Backflow Contamination," *Journal of Spacecraft and Rockets*, Vol. 33, No. 4, 1996, pp. 525–534.

[2]Samanta Roy, R. I., "Numerical Simulation of Ion Thruster Plume Backflow for Spacecraft Contamination Assessment," Ph.D. Thesis, Dept. of Aeronautics and Astronautics, Massachusetts Inst. of Technology, Cambridge, MA, June 1995.

[3]Monheiser, J. M., "Advanced Electric Propulsion Research—1990," NASA CR-187103, May 1991.

[4]Patterson, M., Haag, T., Rawlin, V., and Kussmaul, M., "NASA 30 cm Ion Thruster Development Status," AIAA Paper 94-2849, June 1994.

[5]Patterson, M. J., Haag, T. W., and Hovan, S. A., "Performance of the NASA 30-cm Ion Thruster," International Electric Propulsion Conf., Monterey, CA, Paper 93-108, Sept. 1993.

[6]Brophy, J., private communication, Jet Propulsion Lab., California Inst. of Technology, Pasadena, CA, 1994.

[7]Kaufman, H. R., and Carruth, M. R., "Charge-Exchange Plasma Environment for an Ion Drive Spacecraft," Jet Propulsion Lab., California Inst. of Technology, Publication 79-90, Pasadena, CA, Oct. 1981.

[8]Kemp, R. F., Leudke, E. E., Hall, D. F., and Miller, W. D., "Effects of Electrostatic Rocket Material Deposited on Solar Cells," AIAA Paper 72-447, April 1972.

I. D. Boyd
Associate Editor